THE JOURNAL OF PHYSICAL CHEMISTRY LETTERS
A JOURNAL OF THE AMERICAN CHEMICAL SOCIETY

pubs.acs.org/JPCL

Letter

Spin-Dependent Stereochemistry: A Nonadiabatic Quantum Dynamics Case Study of S + H_2 → SH + H Reaction

Xuezhi Bian* and Joseph E. Subotnik*

Cite This: *J. Phys. Chem. Lett.* 2024, 15, 3434−3440

Read Online

ACCESS | Metrics & More | Article Recommendations | Supporting Information

ABSTRACT: We study the spin-dependent stereodynamics of the S + H_2 → SH + H reaction by using full-dimensional quantum dynamics calculations with zero total nuclear angular momentum along the triplet $^3A''$ states and singlet $^1A'$ states. We find that the interplay between the electronic spin direction and the molecular geometry has a measurable influence on the singlet−triplet intersystem crossing reaction probabilities. Our results show that for some incident scattering angles in the body-fixed frame, the relative difference in intersystem crossing reaction probabilities (as determined between spin up and spin down initial states) can be as large as 15%. Our findings are an *ab initio* demonstration of spin-dependent nonadiabatic dynamics, which we hope will shine light as far as understanding the chiral-induced spin selectivity effect.

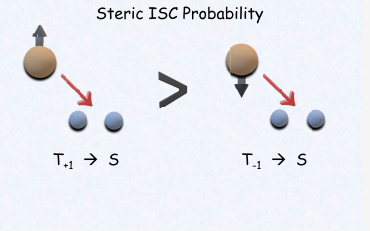

Coupled spin-nuclear-electronic dynamics is a very intriguing research field. In principle, chemists are coming to believe that they can control electronic spin polarization by running a current through a chiral molecule through the chiral-induced spin selectivity (CISS) effect.[1−6] Vice versa, evidence is also emerging that one can engineer chemical reactions by controlling the spin of reaction intermediates (either through CISS[7−9] or simply applying a magnetic field[10]). In both scenarios, the interaction between (nuclear) molecular dynamics and electronic spin plays a pivotal role. However, a theoretical and computational understanding of these coupled dynamics from first-principles is extremely challenging given the number of closely spaced states that must be coupled together (correctly) in a beyond Born−Oppenheimer fashion. For example, even for the simplest singlet−triplet intersystem crossing (ISC) model mediated by spin−orbit coupling (SOC), at least four electronic states are involved, and the three triplets can couple differently to the singlet. While many useful nonadiabatic simulations of ISC have been performed to date, using both wavepacket methods[11−14] and trajectory surface hopping methods,[15−18] very few studies have focused on disentangling the spin-related effects with nuclear dynamics and correlating the geometry of the spin state with chemical outcomes. In other words, for an ISC reaction, there is certainly literature pointing out that a singlet can convert into a triplet (and therefore change molecular geometry), but there is very little written about whether or not that transformation depends on which M_s triplet state (of the three possible triplet states M_s = {1,0,−1}) is produced. Moreover, looking forward, if one is to model such effects, it is essential to go beyond model systems and employ a realistic molecular potentials (ideally *ab initio* potentials) in order to understand practically how spin-dependent nonadiabatic dynamics may or may not control chemical reactions.[19]

One way to address the question above is to focus on stereodynamical scattering. Historically, chemists have recognized that nuclear (usually vibrational) degrees of freedom (DoF) can serve as an efficient way to control chemical reactions,[20−23] and recent experimental advances have focused on stereodynamics−a new promising tool even for nonpolar molecules.[24−28] Within such gas phase scattering experiments, for example, it is known that if one changes the molecular orientation, then one can change the reactivity. For our purposes, we investigate whether there is a connection between the final outcome of a reaction and (i) the nuclear orientation and (ii) the direction of electronic spin polarization just before a reaction.

In this work, to address this question and explore the potential for spin-dependent stereochemistry, we will model the S + H_2 → SH + H insertion reaction. Given that the sulfur atom ground state is a triplet state, we will initialize the incident S atom with different spin polarizations and scan various scattering angles. The S + H_2 → SH + H reaction is an important experimental and theoretical prototype for studying kinetics and dynamics of gas phase bimolecular reactions,[29−33] and previous studies (ref 30) have revealed significant intersystem crossing and nonadiabatic effects. Most importantly, the system is relatively small, which will allow us (i) to utilize high level electronic structure theories (here, multireference configuration interaction (MRCI)) so as to generate accurate global potential energy surfaces (PESs);

Received: November 28, 2023
Revised: February 27, 2024
Accepted: February 28, 2024
Published: March 20, 2024

https://doi.org/10.1021/acs.jpclett.3c03344
J. Phys. Chem. Lett. 2024, 15, 3434−3440

and (ii) to propagate exact full-dimensional nuclear quantum dynamics on these surfaces by the wavepacket method. Overall, the S + H_2 → SH + H system presents an ideal platform for investigating spin-dependent stereodynamics, which is the goal of this Letter.

METHODS

Based on the arguments of Hoffmann, Maiti, and Schatz,[11,12,30] the most important low-energy intersystem crossings for the SHH system are between the singlet $^1A'$ symmetry (where the isolated sulfur atom is S(^{1}D)) and two triplets are of $^3A''$ and $^3A'$ symmetry (and the isolate sulfur atom is S(^{3}P)). By factorizing the electronic wave function into spatial and spin components and applying symmetry arguments, one can reduce this seven-state basis to four states if one cares only about the singlet−triplet ISC dynamics: only three (out of the possible six) triplet states can be coupled directly to the singlet by SOC, namely, $|^3A''(M_s = \pm1)\rangle$ and $|^3A'(M_s = 0)\rangle$, where we define the z-direction to be the direction perpendicular to the triatomic plane. Moreover, in this Letter, we are primarily interested in the $|^3A''(M_s = \pm1)\rangle$ states since the $|^3A'(M_s = 0)\rangle$ state is time-reversal symmetric (and so studying this state cannot yield information about possible spin polarization). Therefore, we further simply the model by considering only the two triplet states ($|^3A''(M_s = \pm1)\rangle$) and the singlet state $^1A'$.

Within a Born−Oppenheimer framework, the three-state intersystem crossing Hamiltonian is given by

$$\hat{H}_{tot} = \hat{T}_n \mathbb{I}_3 + \hat{H}_{ISC} \tag{1}$$

$$\hat{H}_{ISC} = \begin{pmatrix} E_S & V & -V^* \\ V^* & E_T & 0 \\ -V & 0 & E_T \end{pmatrix} \tag{2}$$

Here, T_n is the nuclear kinetic operator, $\mathbb{I}_3$ is a 3 × 3 identity matrix, and E_S and E_T are the energies of the $^1A'$ and $^3A''$ states, respectively. $V = \langle {}^1A'|H_{SO}|{}^3A''(M_s = +1)\rangle$ represents the SOC matrix element between $^1A'$ and $^3A''(M_s = +1)$.

As far defining our reduced space of coordinates, we initialized our system with zero total nuclear angular momentum $\boldsymbol{J}_{nuc} = 0$. The system is then described in the body-fixed (BF) frame by three reactant-based Jacobi coordinates (R, r, and γ) as shown in Figure 1. In such coordinates, the nuclear kinetic operator is of the form:

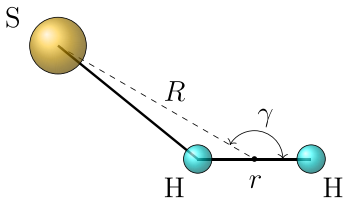

Figure 1. Jacobi coordinates used in this paper for the S + H_2 system. The S atom is scattered toward H_2 molecule with different Jacobi angles γ and initial spin polarizations.

$$\hat{T}_n = -\frac{\hbar^2}{2\mu_R}\frac{\partial^2}{\partial R^2} - \frac{\hbar^2}{2\mu_r}\frac{\partial^2}{\partial r^2} + \frac{\hat{j}^2}{2I} \tag{3}$$

where $\mu_R = \frac{m_S(m_H + m_H)}{(m_S + m_H + m_H)}$ and $\mu_r = \frac{m_H m_H}{m_H + m_H}$ are the reduced masses for Jacobi coordinates R and r, $\hat{j}$ is the nuclear rotational angular momentum operator for H_2 molecule, and $I = (1/\mu_R R^2 + 1/\mu_r r^2)^{-1}$.

The total (nuclear + electronic + spin) wave function can be written as

$$\langle R, r, \gamma|\Psi\rangle = \sum_i \langle R, r, \gamma|\Psi_i\rangle = \sum_i \chi_i(R, r, \gamma)|\psi_i\rangle \tag{4}$$

where χ_i is the nuclear wave function on electronic state $|\psi_i\rangle$ and the index i runs over our three-state spin-diabatic basis $\{S, T_{+1}, T_{-1}\}$. The initial nuclear wave function is expressed as

$$\chi_i(R, r, \gamma, t = 0) = \varphi(R)\,\phi(r)\,u(\gamma) \tag{5}$$

$$\varphi(R) = \left(\frac{1}{\pi\sigma_R}\right)^{1/4} \exp\left(-\frac{(R - R_0)^2}{2\sigma_R^2} - iK_0R\right) \tag{6}$$

Here, the initial average position R_0, initial momentum K_0 and width σ_R together define a localized wavepacket moving in the R direction. Normally, for most scattering calculations, $\phi(r)$ and $u(\gamma)$ are chosen to be the rovibrational eigenstate of the diatomic component of the system. However, in this case, we are interested in stereodynamics scattering and so we will initialize the system in the vibrational ground state ϕ_{v_0} of H_2 with a specific angular distribution (i.e., a Gaussian distribution characterized by γ_0 and σ_γ),

$$\phi(r)\,u(\gamma) = \phi_{v_0}(r)\left(\frac{1}{\pi\sigma_\gamma}\right)^{1/4} \exp\left(-\frac{(\gamma - \gamma_0)^2}{2\sigma_\gamma^2}\right) \tag{7}$$

which allows us to simulate scattering process with different incident scattering angles. Note that our initial setup differs from conventional calculations, where the initial wave function is a single nuclear rotational angular momentum eigenstate. To illustrate this difference, in Figure 2, we have plotted both (left) the spatial angular distribution and (right) the quantum nuclear rotational angular momentum distribution for one particular initial wave function. Although this initial setup may be difficult to achieve experimentally, this approach will yield key insight into spin-dependent stereodynamical effects in chemical reactions.[34]

Ab initio SA-CASSCF/MRCI calculations were carried out so as to generate full-dimensional singlet−triplet ISC potential energy surfaces. For the state-averaged complete active space self-consistent field (SA-CASSCF) calculations, a state-average was employed with equality between three states: the lowest singlet state ($^1A'$) plus the two lowest triplets ($^3A''$ and $^3A'$), all in an aug-cc-pVDZ basis set. The active space contained 8 electrons and 10 active orbitals (9 a' orbitals and 1 a'' orbital). Following the SA-CASSCF calculation, an internally contracted MRCI calculation was performed. Finally, once the MRCI wave functions were computed, we evaluated the spin−orbit coupling matrix elements using the full Breit-Pauli operator.

All electronic structure calculations were performed with the MOLPRO package.[35] To build a potential energy surface, we chose an evenly spaced grid for the R and r coordinates, $0.1a_0 \le R \le 10.0a_0$, $0.1a_0 \le r \le 10.0a_0$, with $N_R = 400$ and $N_r = 100$. For the coordinate $\gamma \in [0, \pi]$, we chose the discretization as follows. First, we sampled $\cos(\gamma)$ from a standard set of Gauss−Legendre quadrature points on $[-1, 1]$ for $N_\gamma = 100$, $\{x_1, x_2, ..., x_{N_\gamma}\}$;

https://doi.org/10.1021/acs.jpclett.3c03344
J. Phys. Chem. Lett. 2024, 15, 3434−3440

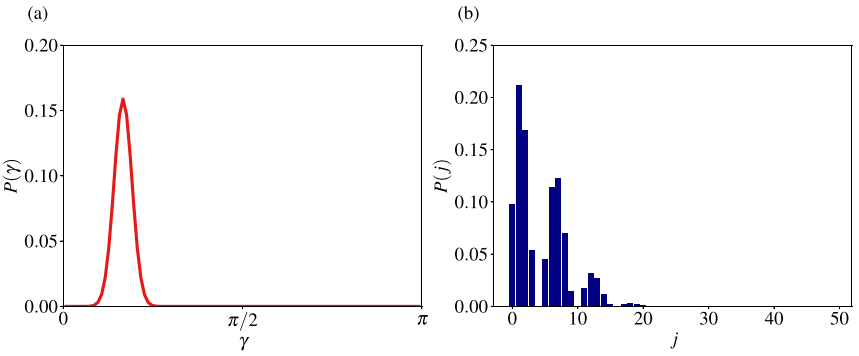

Figure 2. (a) Spatial distribution as a function of Jacobi angle γ for an initial wave packet with $\gamma_0 = \pi/6$ and $\sigma_\gamma = \pi/20$. (b) Corresponding quantum nuclear rotational angular momentum distribution for the same initial wave packet.

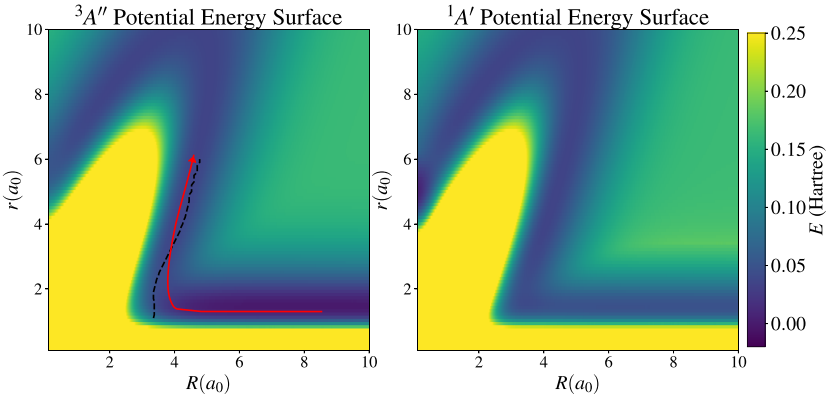

Figure 3. Colormap plot depicting the PES of $^3A''$ state for a constant Jacobi angle $\gamma = \pi/6$. The wavepacket will go through the singlet−triplet ISC seam (the black dashed curve) along the reaction path (the red curve with an arrow) from the S/H_2 basin to the SH/H basin.

second, we inverted these points with the cosine function, $\gamma_j = \cos^{-1}(x_j)$. The points sampled above are used directly as grid points for propagating our quantum wave packet dynamics below, and no interpolation is performed. In Figure 3, we show a plot of the $^3A''$ PES for a fixed angle $\gamma = \pi/6$. All energies are relative to the reactant asymptotic energy.

In Figure 3, we also show a simple low-energy path in configuration space from the S/H_2 basin to the SH/H basin; the singlet−triplet ISC seam is also shown. The nuclear wavepacket is initialized when the S atom and H_2 molecule are far apart (large R) on the triplet electronic PES, and one can imagine the S atom being scattered toward H_2 along the red curve in Figure 3). Following the path in red, a nuclear wavepacket passes through the singlet−triplet ISC seam (the black dashed curve).

As mentioned above, we enforced zero total nuclear angular momentum values for our simulations. At time zero, the nuclear wavepackets are initialized on one of the pure triplet spin-diabatic states T_{+1} or T_{-1} at $R_0 = 6.0a_0$ with $\sigma_R = 0.5a_0$. The initial momentum was set to be $K_0 = -25.0$ au (see eq 6). Dynamical calculations were run for different γ_0 values (see eq 7), but the angular distribution had a fixed width, $\sigma_\gamma = \pi/20$. For more details of our three-dimensional wavepacket calculations, please see the Supporting Information.

To compute the final reaction probability, we calculated the cumulative probability flux for a dividing surface at $r_s = 5a_0$,

$$P_i = \frac{\hbar}{\mu_{H_2}} \int_0^{+\infty} dt \mathrm{Im}(\langle \Psi_i(t)|\delta(r = r_s)\nabla_r|\Psi_i(t)\rangle) \quad (8)$$

Here, we evaluated $\nabla_r|\Psi\rangle$ with a Fourier transformation. In Figure 4, we plot the cumulative reaction probability $P_{T_{\pm 1}\to S}$ from

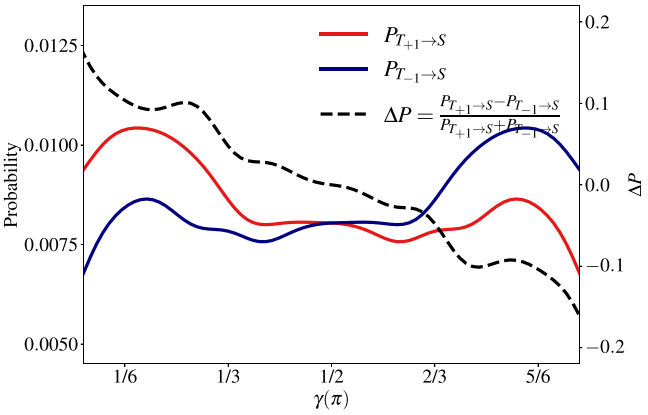

Figure 4. Reaction probabilities from triplets T_{+1} and T_{-1} to the singlet S with an incident energy of 0.1 hartree are plotted as a function of incident Jacobi angles γ, demonstrating steoredynamical effects. Furthermore, distinct ISC reaction probabilities emerge when systems are initialized with different spin-polarization at the same scattering angle.

state T_{+1} or T_{+1} to state S as well as the relative "spin-polarized probability" $\Delta P = \frac{P_{T_{+1}\to S} - P_{T_{-1}\to S}}{P_{T_{+1}\to S} + P_{T_{-1}\to S}}$ for various incident scattering angles in the BF frame. We find that the ISC reaction probabilities clearly exhibit stereodynamic effects that are dependent on the incident scattering angle and initial spin state. Note that even though the total probability for a triplet to transform to a singlet is small, the relative difference between $P_{T_{+1}\to S}$ and $P_{T_{-1}\to S}$ can be as large as 15% for small incident

https://doi.org/10.1021/acs.jpclett.3c03344
J. Phys. Chem. Lett. 2024, 15, 3434−3440

angles. Note also that the reaction probabilities for two spin polarization show a symmetry around $\gamma = \pi/2$; more precisely, $P_{T_{+1}\to S}(\gamma) = P_{T_{-1}\to S}(\pi - \gamma)$. As shown in Figure 5, this

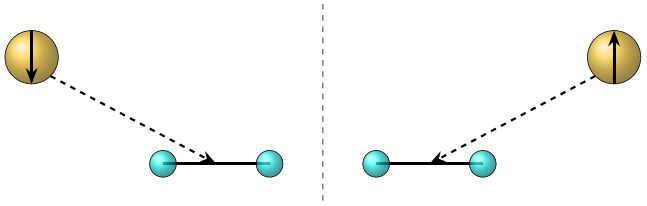

Figure 5. Upon a mirror reflection of the total system as shown in the figure, the incident Jacobi angle changes from γ to $\pi - \gamma$ and the electronic spin is reversed. The ISC dynamics will be identical before and after this transformation.

symmetry can be easily understood by considering a mirror reflection along the axis perpendicular to the diatomic bond with a corresponding reversal of spin-state. By considering the scenarios in Figure 5 from different viewpoints, one must conclude that both scenarios lead to the same dynamics and reaction probabilities. As a result, when the system begins with C_{2v} symmetry, i.e., $\gamma = \pi/2$, it follows that the ISC reaction probabilities must be identical and there can be no spin-polarization, as shown in Figure 4. Also, it is not hard to deduce that the spin-dependent reaction probabilities $P_{T_{+1}\to S}$ and $P_{T_{-1}\to S}$ for systems initialized from any of the diatomic rotational eigenstates will be the same.

Another quantity of interest is the energy-resolved reaction probability $P_i(E)$,[36]

$$P_i(E) = \frac{\hbar}{\mu_{H_2}} \mathrm{Im}(\langle \Psi_i(E)|\delta(r = r_s)\nabla_r|\Psi_i(E)\rangle) \tag{9}$$

$$|\Psi_i(E)\rangle = \frac{1}{a(E)} \int_0^{+\infty} \mathrm{d}t e^{iEt}|\Psi_i(t)\rangle \tag{10}$$

where $|\Psi_i(E)\rangle$ is calculated from a Fourier transform and $a(E)$ is the energy E component of the initial nuclear wavepacket. As illustrated in Figure 6, the probability of the ISC reaction for an incident angle of $\gamma = \pi/6$ varies for the two different initial spin polarizations over a range of energies. However, the reaction probability for reaching a singlet when starting from state T_{+1} is larger than when starting from state T_{-1} for most energies, including the intermediate incident energy, $E \approx 0.1$ hartree. Thus, the data in Figure 6 are consistent with the data in Figure 4. It is also prudent now to consider the extreme cases of low and high incoming energy. At low incident energy, $E < 0.04$ hartree, the nuclear wavepacket does not have enough energy to pass the triplet barrier so the reaction probability is close to 0. At very high energy, the dynamics become more diabatic and the wavepacket tends to stay on the same triplet spin-diabat and the ISC reaction probability vanishes.

Discussion: In the present work, we have analyzed if and how the S + H_2 → SH + H insertion reaction may lead to spin-dependent stereodynamical effects. Our results show a measurable spin preference (∼10%) for the intersystem crossing reaction probabilities at certain geometries. Given the fact that singlet−triplet ISCs are ubiquitous and energetically accessible in numerous molecular systems, this finding should be of interest as spin-dependent effects may well exist for many other reactions (with much larger molecules). However, before we dive into *ab initio* or experimental investigations of more complicated systems, several points are worth mentioning.

To begin with, we note first that although the scattering products must depend sensitively on the nuclear orientation (or Jacobi angle γ) of incidence, meaningful statistics can always be (and were) extracted by looking at the differences between results for different spin states; moreover, given the fact that initial reactants are nonpolar, steering effects are not completely dominant here as far as the ISC channel. Second, although there is a meaningful *relative* difference in the spin-dependent reactivities, we found that the total ISC probability is rather small (only ∼1%) on an absolute scale for the current theoretical scattering setup. To amplify the spin-dependent ISC probability, one should consider systems with larger SOC (e.g., molecules that contain heavier atoms). More interestingly, one can also consider systems in the condensed phase with more scattering events; after all, excited triplets are more energetically favorable than excited singlets and, with more scattering events and a faster drive to equilibrate, one can suppose that triplet populations will increase (and one can investigate possible triplet spin polarization) with more triplet states available. For both of these scenarios, the size of the calculation will be larger, with more nuclear and electronic DoFs, and as such, exact quantum dynamics will likely not be viable and we will need to use a semiclassical framework.

To that end, we have explored the S + H_2 → SH + H system above using a naive version of Tully's fewest switches surface hopping (FSSH) method. The FSSH simulations are propagated on a spin-diabatic basis with cubic-spline interpolated potential energy surfaces. In Figure 7, we plot the ISC reaction probabilities calculated from FSSH method. For each data point, 10^6 trajectories are sampled from the same initial

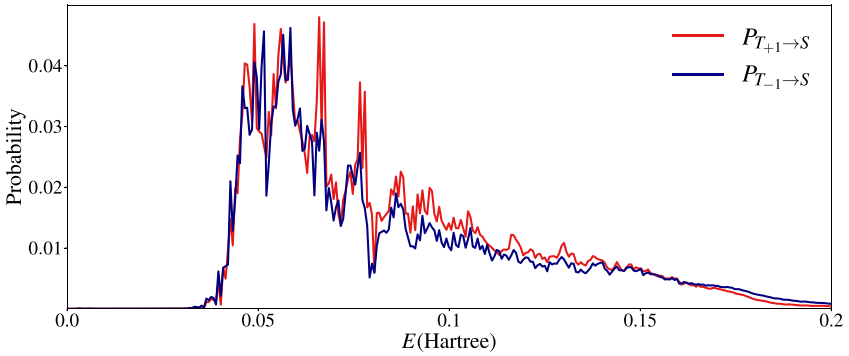

Figure 6. Energy-resolved reaction probabilities for systems initialized on T_{+1} and T_{-1} with incident scattering angle $\gamma = \pi/6$.

https://doi.org/10.1021/acs.jpclett.3c03344
J. Phys. Chem. Lett. 2024, 15, 3434−3440

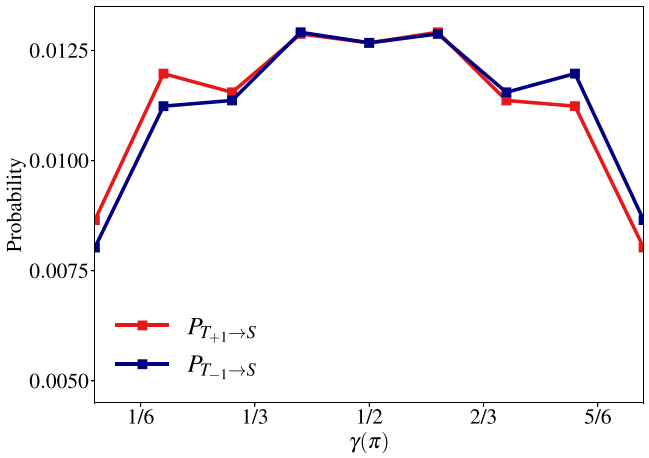

Figure 7. Reaction probabilities calculated from naive spin-diabatic surface hopping method.

conditions as in Figure 4. We rescale the momentum along the direction of the difference of diabatic gradients $\vec{\lambda}_{jk} = \nabla E_j - \nabla E_k$ when trajectories hop between surface j and k. We note that the results of the ISC reaction probability are quite sensitive to the momentum rescaling directions (see below), but overall, according to Figure 7, naive FSSH gives results that qualitatively agree with the wavepacket results. We find a similar spin-polarized pattern as a function of incident scattering angle comparing to the quantum results, which suggests that FSSH-like methods can serve as effective approaches for investigating spin-dependent nonadiabatic dynamics, which is a growing field of study nowadays.

To understand how this spin asymmetry arises within surface hopping, note that there is only one possibility: spin polarization emerges when the distinct coupling matrix elements in the electronic Hamiltonian described in eq 2 lead to different quantum amplitudes. In other words, the different SOC matrix elements that couple T_{+1} and T_{-1} to S will lead to different hopping probabilities between these spin states and, as Figure 7 shows, these probabilities can be reasonably accurate. This finding is of particular interest because spin-diabatic FSSH does not conserve the total angular momentum for several reasons: (i) Hopping between states often produces changes in angular momentum depending on the rescaling direction.[37] As a practical note, we mention that if we employed a different momentum rescaling direction, e.g., $\vec{\lambda}_{jk} = \mathrm{Re}(\nabla \mathrm{H}_{\mathrm{jk}})$ and $\vec{\lambda}_{jk} = \mathrm{Im}(\nabla H_{jk})$, our results were far worse compared to exact quantum calculations. Interestingly, here we have rescaled momenta in the direction of the gradient of the different diabatic energies, $\nabla E_j - \nabla E_k$. Moreover, for any closed isotropic system, it is very easy to show that $\boldsymbol{R} \times \boldsymbol{F}_j = 0$. Thus, it follows that

$$\frac{d\boldsymbol{J}_{\mathrm{nuc}}}{dt} = \boldsymbol{R} \times \boldsymbol{F}_j = 0 \tag{11}$$

Thus, the present algorithm does, in fact, conserve nuclear angular momenta, which might partially explain our good results here.

(ii) A second and more serious obstacle is that whenever classical Born−Oppenheimer dynamics are run along an isotropic surface, one conserves only the *nuclear* angular momentum and not the *total* nuclear plus spin plus electronic (as computed by the amplitudes) angular momentum, which must cast some doubt on running spin-diabatic FSSH dynamics. Now, one usually performs FSSH in an adiabatic (rather than diabatic) basis[38] and over the past few years, there has been a push to understand how to propagate adiabatic FSSH dynamics with spin DoF. One key ingredient arises in such a case: nuclear Berry curvature effects.[39,40] When running classical dynamics, such nuclear Berry curvature effects induce a pseudomagnetic field for the nuclear motion that in turn alters trajectories, leading to angular momentum transfer between nuclei and electronic components and ultimately enforcing *total* angular momentum conservation.[41] These effects do not arise within spin-diabatic FSSH calculations, where the diabatic potential energy surfaces of T_{+1} and T_{-1} are identical, and one always finds identical nuclear motion along both. Incorporating nuclear Berry curvature effects within semiclassical dynamics methods (especially FSSH) is a nontrivial task, and developing meaningful algorithms for doing so will be an important step toward a quantitative understanding of spin-dependent nonadiabatic dynamics in more general/complicated systems.[42,43]

Lastly, let us go beyond the FSSH framework and consider the origin of this spin-dependency from a more general physical perspective. Quite generally, generating spin-dependent reaction products requires two ingredients−time-reversal symmetry breaking and spatial inversion symmetry breaking.[44] The need for time-reversal symmetry breaking can be understood from the first-order perturbation theory. At equilibrium, the ISC Fermi Golden Rule rates $k_{\mathrm{FGR}} = 2\pi/\hbar\,|\langle T_{\pm 1}|H_{\mathrm{ISC}}|S\rangle|^2$ are identical for the two triplet spin-diabats, which implies that introducing spin polarization must be a nonequilibrium property. In our calculations, the system exhibits strong nonequilibrium features by construction: we are running scattering calculations. It will be very interesting to assess if/how spin polarization emerges in the condensed phase, e.g., in electron transfer problems, where equilibration occurs more quickly and the environment must be considered very carefully. Next, the need for spatial inversion symmetry breaking can be analogously understood in the context of the condensed matter theory. Periodic electronic structure calculations with Rashba[45] and Dresselhaus[46] coupling make clear that the spin components of electronic bands can split apart for systems without spatial inversion symmetry. As far as our present calculations are concerned, we recovered spin polarization only when we resolved the scattering event over different incident Jacobi angles, γ; if we were to average over γ, and assume an isotropic distribution of incoming angles, we would not see any spin polarization. Thus, if an experimentalists aims to see the ISC spin polarization we observe here for a scattering experiment, it will be crucial to align all the molecules in the laboratory frame, which can presumably be achieved by employing laser techniques in ultracold experiments[47,48] or attaching molecules to a surface.[49]

As a side note, before concluding, one more point about the S + H_2 system is appropriate. The presented three-dimensional quantum dynamics simulations can still be improved on at least **two** aspects: (i) Here, we have considered only systems with a zero total nuclear angular momentum. More generally, for systems with nonzero total nuclear angular momentum, one must include four nuclear DoFs (the three included above and the projection of total nuclear angular momentum in the body-fixed z-axis J^z_{nuc}) and consider Coriolis couplings between different J^z_{nuc} states. (ii) Our dynamics here go beyond electrostatic Born−Oppenheimer calculations and the presence of spin−orbit coupling changes the electronic spin angular

https://doi.org/10.1021/acs.jpclett.3c03344
J. Phys. Chem. Lett. 2024, 15, 3434−3440

momentum for a system with both singlet and triplet character. Thus, if one wished to describe the S + H_2 dynamics exactly, then one would need formally to include as a degree of freedom the total *nuclear* angular momentum $\boldsymbol{J}_{nuc}$ (which is not a good quantum number for systems with SOC). Implementing such five dimensional simulations and exploring the subsequent molecular scattering dynamics remains another future research direction if one is interested in the most accurate possible bimolecular scattering reactions.

In summary, we discussed how spin-dependent reaction probabilities can and do emerge for a well-known ISC problem in chemical physics. We find three ingredients are necessary for realizing spin-dependent chemical reactivity: spin−orbit coupling, time-reversal symmetry breaking, and spatial inversion symmetry breaking. Interestingly, naive spin-diabatic mixed quantum classical FSSH calculations are qualitatively accurate for the dynamics investigated here, but as mentioned above, that may be coincidental: the FSSH calculations here do conserve nuclear angular momentum but mostly ignore the transfer of angular momentum between electronic and nuclear degrees of freedom.

Looking forward, the subject of angular momentum transfer and conservation is directly relevant to the CISS phenomenon, and the present results suggest semiclassical approaches should be helpful studying larger systems (with more than three atoms) in the future. In particular, given the significance of nuclear motion in the incoherent charge transfer mechanism observed in organic molecules like DNA[50,51] where a CISS effect is observed, as well as the temperature dependence observed within CISS experiments,[52,53] there is a very strong reason to further develop mixed-quantum classical calculations that do treat spins, electrons, and nuclei consistently. Since the present calculations clearly reveal measurable spin-dependent effects for small systems, one wonders if simulations on larger systems will reveal larger effects, potentially helping to understand and explain CISS.

■ ASSOCIATED CONTENT

Supporting Information

The Supporting Information is available free of charge at https://pubs.acs.org/doi/10.1021/acs.jpclett.3c03344.

Additional details of wave packet dynamics simulations and some one-dimensional cuts of the potential energy surface (PDF)

■ AUTHOR INFORMATION

Corresponding Authors

Xuezhi Bian − *Department of Chemistry, University of Pennsylvania, Philadelphia, Pennsylvania 19104, United States*; orcid.org/0000-0001-6445-7462; Email: xzbian@sas.upenn.edu

Joseph E. Subotnik − *Department of Chemistry, University of Pennsylvania, Philadelphia, Pennsylvania 19104, United States*; Email: subotnik@sas.upenn.edu

Complete contact information is available at: https://pubs.acs.org/10.1021/acs.jpclett.3c03344

Notes

The authors declare no competing financial interest.

The source code of our potential energy surface is available on GitHub at https://github.com/xzbian/H2S.

■ ACKNOWLEDGMENTS

This work has been supported by the U.S. Department of Energy, Office of Science, Office of Basic Energy Sciences, under Award no. DE-SC0019397 (J.E.S.). X.B. thanks Yanze Wu for numerous helpful discussions.

■ REFERENCES

(1) Ray, K.; Ananthavel, S.; Waldeck, D.; Naaman, R. Asymmetric scattering of polarized electrons by organized organic films of chiral molecules. *Science* **1999**, *283*, 814−816.

(2) Göhler, B.; Hamelbeck, V.; Markus, T.; Kettner, M.; Hanne, G.; Vager, Z.; Naaman, R.; Zacharias, H. Spin selectivity in electron transmission through self-assembled monolayers of double-stranded DNA. *Science* **2011**, *331*, 894−897.

(3) Naaman, R.; Waldeck, D. H. Chiral-induced spin selectivity effect. *journal of physical chemistry letters* **2012**, *3*, 2178−2187.

(4) Naaman, R.; Paltiel, Y.; Waldeck, D. H. Chiral molecules and the electron spin. *Nature Reviews Chemistry* **2019**, *3*, 250−260.

(5) Naaman, R.; Paltiel, Y.; Waldeck, D. H. Chiral induced spin selectivity gives a new twist on spin-control in chemistry. *Acc. Chem. Res.* **2020**, *53*, 2659−2667.

(6) Eckvahl, H. J.; Tcyrulnikov, N. A.; Chiesa, A.; Bradley, J. M.; Young, R. M.; Carretta, S.; Krzyaniak, M. D.; Wasielewski, M. R. Direct observation of chirality-induced spin selectivity in electron donor−acceptor molecules. *Science* **2023**, *382*, 197−201.

(7) Mtangi, W.; Kiran, V.; Fontanesi, C.; Naaman, R. Role of the electron spin polarization in water splitting. *journal of physical chemistry letters* **2015**, *6*, 4916−4922.

(8) Ghosh, S.; Bloom, B. P.; Lu, Y.; Lamont, D.; Waldeck, D. H. Increasing the efficiency of water splitting through spin polarization using cobalt oxide thin film catalysts. *J. Phys. Chem. C* **2020**, *124*, 22610−22618.

(9) Vadakkayil, A.; Clever, C.; Kunzler, K. N.; Tan, S.; Bloom, B. P.; Waldeck, D. H. Chiral electrocatalysts eclipse water splitting metrics through spin control. *Nat. Commun.* **2023**, *14*, 1067.

(10) Steiner, U. E.; Ulrich, T. Magnetic field effects in chemical kinetics and related phenomena. *Chem. Rev.* **1989**, *89*, 51−147.

(11) Hoffmann, M. R.; Schatz, G. C. Theoretical studies of intersystem crossing effects in the O + H2 reaction. *J. Chem. Phys.* **2000**, *113*, 9456−9465.

(12) Maiti, B.; Schatz, G. C. Theoretical studies of intersystem crossing effects in the O(3P, 1D) + H2 reaction. *J. Chem. Phys.* **2003**, *119*, 12360−12371.

(13) Wang, Y.; Guo, H.; Yarkony, D. R. Internal conversion and intersystem crossing dynamics based on coupled potential energy surfaces with full geometry-dependent spin−orbit and derivative couplings. Nonadiabatic photodissociation dynamics of NH3 (A) leading to the NH (X3Σ-, a1Δ) + H2 channel. *Phys. Chem. Chem. Phys.* **2022**, *24*, 15060−15067.

(14) Guan, Y.; Xie, C.; Guo, H.; Yarkony, D. R. Toward a Unified Analytical Description of Internal Conversion and Intersystem Crossing in the Photodissociation of Thioformaldehyde. I. Diabatic Singlet States. *J. Chem. Theory Comput.* **2023**, *19*, 6414−6424.

(15) Tully, J. C. Molecular dynamics with electronic transitions. *J. Chem. Phys.* **1990**, *93*, 1061−1071.

(16) Cui, G.; Thiel, W. Generalized trajectory surface-hopping method for internal conversion and intersystem crossing. *J. Chem. Phys.* **2014**, *141*, No. 124101.

(17) Mai, S.; Marquetand, P.; González, L. A general method to describe intersystem crossing dynamics in trajectory surface hopping. *Int. J. Quantum Chem.* **2015**, *115*, 1215−1231.

(18) Zaari, R. R.; Varganov, S. A. Nonadiabatic transition state theory and trajectory surface hopping dynamics: intersystem crossing between 3B1 and 1A1 states of SiH2. *J. Phys. Chem. A* **2015**, *119*, 1332−1338.

(19) Bian, X.; Wu, Y.; Teh, H.-H.; Zhou, Z.; Chen, H.-T.; Subotnik, J. E. Modeling nonadiabatic dynamics with degenerate electronic states, intersystem crossing, and spin separation: A key goal for chemical physics. *J. Chem. Phys.* **2021**, *154*, No. 110901.

(20) Schatz, G. C.; Colton, M. C.; Grant, J. L. A quasiclassical trajectory study of the state-to-state dynamics of atomic H + H2O → OH + H2. *J. Phys. Chem.* **1984**, *88*, 2971−2977.
(21) Sinha, A.; Hsiao, M. C.; Crim, F. F. Bond-selected bimolecular chemistry: H + HOD (4νOH) → OD + H2. *J. Chem. Phys.* **1990**, *92*, 6333−6335.
(22) Guettler, R. D.; Jones Jr, G. C.; Posey, L. A.; Zare, R. N. Partial control of an ion−molecule reaction by selection of the internal motion of the polyatomic reagent ion. *Science* **1994**, *266*, 259−261.
(23) Zare, R. N. Laser control of chemical reactions. *science* **1998**, *279*, 1875−1879.
(24) Loesch, H.; Remscheid, A. Brute force in molecular reaction dynamics: A novel technique for measuring steric effects. *J. Chem. Phys.* **1990**, *93*, 4779−4790.
(25) Aldegunde, J.; de Miranda, M. P.; Haigh, J. M.; Kendrick, B. K.; Sáez-Rábanos, V.; Aoiz, F. J. How reactants polarization can be used to change and unravel chemical reactivity. *J. Phys. Chem. A* **2005**, *109*, 6200−6217.
(26) Liu, K. Vibrational control of bimolecular reactions with methane by mode, bond, and stereo selectivity. *Annu. Rev. Phys. Chem.* **2016**, *67*, 91−111.
(27) Wang, Y.; Huang, J.; Wang, W.; Du, T.; Xie, Y.; Ma, Y.; Xiao, C.; Zhang, Z.; Zhang, D. H.; Yang, X. Stereodynamical control of the H + HD → H2 + D reaction through HD reagent alignment. *Science* **2023**, *379*, 191−195.
(28) Yang, C.; Li, Y.; Zhou, S.; Guo, Y.; Jia, C.; Liu, Z.; Houk, K. N.; Dubi, Y.; Guo, X. Real-time monitoring of reaction stereochemistry through single-molecule observations of chirality-induced spin selectivity. *Nat. Chem.* **2023**, *15*, 972−979.
(29) Zhang, H.; Smith, S. C. Lanczos Subspace Time-Independent Wave Packet Calculations of S(1D) + H2 Reactive Scattering. *J. Phys. Chem. A* **2002**, *106*, 6137−6142.
(30) Maiti, B.; Schatz, G. C.; Lendvay, G. Importance of intersystem crossing in the S (3P, 1D)+ H2 → SH+ H reaction. *J. Phys. Chem. A* **2004**, *108*, 8772−8781.
(31) Chu, T.-S.; Han, K.-L.; Schatz, G. C. Significant nonadiabatic effects in the S (1D) + HD reaction. *J. Phys. Chem. A* **2007**, *111*, 8286−8290.
(32) Berteloite, C.; Lara, M.; Bergeat, A.; Le Picard, S. D.; Dayou, F.; Hickson, K. M.; Canosa, A.; Naulin, C.; Launay, J.-M.; Sims, I. R.; et al. Kinetics and Dynamics of the S(1D2) + H2 → SH + H Reaction at Very Low Temperatures and Collision Energies. *Phys. Rev. Lett.* **2010**, *105*, No. 203201.
(33) Duan, Z. X.; Li, W. L.; Xu, W. W.; Lv, S. J. Quasiclassical dynamics for the H + HS abstraction and exchange reactions on the 3A" and the 3A' states. *J. Chem. Phys.* **2013**, *139*, No. 094307.
(34) As a practical matter, there is a nuance which may make this setup difficult to achieve. Note that, because we have assumed that the total nuclear angular momentum $J = 0$ in eq 3, the distribution of nuclear rotational angular momentum j sampled in Figure 2 must be compensated by the nuclear orbital angular momentum of the atom−diatom system in order to apply the theory stemming from eq 3, and achieving such a superposition of initial states may be difficult in practice. In other words, the resulting nuclear wave functions from eq 7 are not equivalent to a diatomic pendular state, which is usually constructed as a superposition of rotational angular momentum eigenstates with different total nuclear angular momenta.
(35) Werner, H.-J.; Knowles, P. J.; Manby, F. R.; Black, J. A.; Doll, K.; Heßelmann, A.; Kats, D.; Köhn, A.; Korona, T.; Kreplin, D. A.; et al. The Molpro quantum chemistry package. *J. Chem. Phys.* **2020**, *152*, No. 144107.
(36) Zhang, D. H.; Zhang, J. Z. Quantum reactive scattering with a deep well: Time-dependent calculation for H + O2 reaction and bound state characterization for HO2. *J. Chem. Phys.* **1994**, *101*, 3671−3678.
(37) Shu, Y.; Zhang, L.; Varga, Z.; Parker, K. A.; Kanchanakungwankul, S.; Sun, S.; Truhlar, D. G. Conservation of angular momentum in direct nonadiabatic dynamics. *J. Phys. Chem. Lett.* **2020**, *11*, 1135−1140.
(38) Tully, J. Mixed quantum−classical dynamics. *Faraday Discuss.* **1998**, *110*, 407−419.
(39) Miao, G.; Bellonzi, N.; Subotnik, J. An extension of the fewest switches surface hopping algorithm to complex Hamiltonians and photophysics in magnetic fields: Berry curvature and "magnetic" forces. *J. Chem. Phys.* **2019**, *150*, No. 124101.
(40) Takatsuka, K. Lorentz-like force emerging from kinematic interactions between electrons and nuclei in molecules: A quantum mechanical origin of symmetry breaking that can trigger molecular chirality. *J. Chem. Phys.* **2017**, *146*, 084312.
(41) Bian, X.; Tao, Z.; Wu, Y.; Rawlinson, J.; Littlejohn, R. G.; Subotnik, J. E. Total angular momentum conservation in ab initio Born-Oppenheimer molecular dynamics. *Phys. Rev. B* **2023**, *108*, L220304.
(42) Bian, X.; Wu, Y.; Teh, H.-H.; Subotnik, J. E. Incorporating Berry force effects into the fewest switches surface-hopping algorithm: Intersystem crossing and the case of electronic degeneracy. *J. Chem. Theory Comput.* **2022**, *18*, 2075−2090.
(43) Bian, X.; Wu, Y.; Rawlinson, J.; Littlejohn, R. G.; Subotnik, J. E. Modeling spin-dependent nonadiabatic dynamics with electronic degeneracy: a phase-space surface-hopping method. *J. Phys. Chem. Lett.* **2022**, *13*, 7398−7404.
(44) Zöllner, M. S.; Varela, S.; Medina, E.; Mujica, V.; Herrmann, C. Insight into the origin of chiral-induced spin selectivity from a symmetry analysis of electronic transmission. *J. Chem. Theory Comput.* **2020**, *16*, 2914−2929.
(45) Rashba, E. Properties of semiconductors with an extremum loop. I. Cyclotron and combinational resonance in a magnetic field perpendicular to the plane of the loop. *Sov. Phys.-Solid State* **1960**, *2*, 1109.
(46) Dresselhaus, G. Spin-orbit coupling effects in zinc blende structures. *Phys. Rev.* **1955**, *100*, 580.
(47) Rost, J.; Griffin, J.; Friedrich, B.; Herschbach, D. Pendular states and spectra of oriented linear molecules. *Physical review letters* **1992**, *68*, 1299.
(48) Mukherjee, N.; Dong, W.; Zare, R. N. Coherent superposition of M-states in a single rovibrational level of H2 by Stark-induced adiabatic Raman passage. *J. Chem. Phys.* **2014**, *140*, No. 074201.
(49) Yoder, B. L.; Bisson, R.; Beck, R. D. Steric effects in the chemisorption of vibrationally excited methane on Ni (100). *Science* **2010**, *329*, 553−556.
(50) Xiang, L.; Palma, J. L.; Bruot, C.; Mujica, V.; Ratner, M. A.; Tao, N. Intermediate tunnelling−hopping regime in DNA charge transport. *Nature Chem.* **2015**, *7*, 221−226.
(51) Kim, H.; Kilgour, M.; Segal, D. Intermediate coherent−incoherent charge transport: DNA as a case study. *J. Phys. Chem. C* **2016**, *120*, 23951−23962.
(52) Das, T. K.; Tassinari, F.; Naaman, R.; Fransson, J. Temperature-dependent chiral-induced spin selectivity effect: Experiments and theory. *J. Phys. Chem. C* **2022**, *126*, 3257−3264.
(53) Alwan, S.; Sarkar, S.; Sharoni, A.; Dubi, Y. Temperature-dependence of the chirality-induced spin selectivity effect—Experiments and theory. *J. Chem. Phys.* **2023**, *159*, No. 014106.

https://doi.org/10.1021/acs.jpclett.3c03344
J. Phys. Chem. Lett. 2024, 15, 3434−3440